The Mechanism for Isopenicillin N Synthase from Density-Functional Modeling Highlights the Similarities with Other Enzymes in the 2-His-1-carboxylate Family†

Marcus Lundberg,‡ Per E. M. Siegbahn,§ and Keiji Morokuma*,‡

Fukui Institute for Fundamental Chemistry, Kyoto University, 34-4 Takano Nishihiraki-cho, Sakyo, Kyoto 606-8103, Japan, and Department of Physics, Quantum Chemistry Group, Stockholm University, SE-106 91 Stockholm, Sweden

Received August 7, 2007; Revised Manuscript Received October 3, 2007

ABSTRACT: Isopenicillin N synthase (IPNS) catalyzes a key step in the biosynthesis of the important β-lactam antibiotics penicillins and cephalosporins. Density-functional calculations with the B3LYP functional are used to propose a detailed mechanism for this reaction. The results support the general scheme outlined from experimental observations, with formation of a four-membered β-lactam ring followed by formation of a five-membered thiazolidine ring. However, an alternative mechanism for the heterolytic O−O bond cleavage and β-lactam ring formation steps is proposed. The former part involves protonation of the distal oxygen by an iron-bound water ligand. This mechanism highlights the strong similarities that exist between IPNS and other enzymes of the 2-histidine-1-carboxylate family, especially pterin-dependent amino acid hydroxylases and α-keto acid-dependent dioxygenases. Both activation of the cysteine β-C−H bond by an iron-bound superoxo radical and activation of the valine β-C−H bond by a ferryl−oxo species show reaction barriers close to the experimentally measured one. These results are in agreement with kinetic isotope experiments that suggest both C−H bond activation steps to be partially rate limiting. The ring formation sequence is determined by the relative strengths of the two C−H bonds. Only the ferryl−oxo intermediate is capable of activating the stronger valine β-C−H bond.

Isopenicillin N synthase (IPNS)[1] catalyzes the formation of isopenicillin N, a key step in the synthesis of the important β-lactam antibiotics penicillins and cephalosporins (*1*−*4*). Because an efficient fully synthetic route to isopenicillin N is missing, the biosynthesis reaction is still used in large-scale production. The enzyme is a potential target in the design of novel antibiotic compounds (*5*). Theoretical modeling improves our understanding of the requirements for successful biosynthesis and can be a guide for substrate modification and/or protein engineering.

IPNS belongs to a family of oxygen-activated mononuclear non-heme iron enzymes with the 2-histidine-1-carboxylate binding motif. Other enzymes in the same family are pterin-dependent hydroxylases, α-keto acid-dependent dioxygenases, Rieske dioxygenases, and extradiol dioxygenases (*6*, *7*). IPNS uses the four-electron oxidative power of O_2 to catalyze the transformation of the linear tripeptide substrate δ-(L-α-aminoadipoyl)-L-cysteinyl-D-valine (ACV) to isopenicillin N (IPN) (see Scheme 1). IPN is bicyclic with a four-membered β-lactam ring and a five-membered thiazolidine ring.

Compared to other reactions in the same enzymatic family, the substrate reaction in IPNS has a few unique features. IPNS is, together with 1-aminocyclopropane-1-carboxylic acid oxidase (ACCO), the only enzyme in this family in which all four electrons required to reduce dioxygen come from the substrate (*8*). In addition, no oxygen atom is incorporated into the substrate. Instead, abstraction of four substrate hydrogens, highlighted in Scheme 1, leads to the formation of two water molecules.

A proposal for the enzymatic mechanism of IPNS (*4*) has been formulated on the basis of incubation (*2*), spectroscopic (*9*−*11*), and crystallographic studies of substrate and substrate analogues (*4*, *12*−*17*) (see Scheme 2). Binding of the ACV substrate results in a five-coordinate iron site where iron is ligated by His214, Asp216, His270 (*Aspergillus nidulans* numbering), the substrate thiolate, and one water molecule (*4*). Although there are many highly conserved residues in IPNS, the three iron ligands are so far the only ones that seem to be critical for activity (the D216E mutation retains 1% activity) (*18*−*20*). Iron is in the high-spin Fe(II) state ($S = 2$) (*9*). This is the preferred spin state for this family of enzymes and reflects the weak ligand field of the coordinating amino acids (*21*).

Substrate binding increases the enzyme's affinity for oxygen, either by increasing the hydrophobicity of the active

†M.L. acknowledges a Fukui Institute for Fundamental Chemistry fellowship. This work was in part supported by a CREST (Core Research for Evolutional Science and Technology) grant in the Area of High Performance Computing for Multi-scale and Multi-physics Phenomena from the Japan Science and Technology Agency (JST).

* To whom correspondence should be addressed. E-mail: morokuma@fukui.kyoto-u.ac.jp. Telephone: +81-75-711-7843. Fax: +81-75-781-4757.

‡ Kyoto University.

§ Stockholm University.

[1] Abbreviations: ACCO, 1-aminocyclopropane-1-carboxylic acid oxidase; ACmC, δ-(L-α-aminoadipoyl)-L-cysteinyl-L-*S*-methylcysteine; ACV, δ-(L-α-aminoadipoyl)-L-cysteinyl-D-valine; B3LYP, Becke's three-parameter exchange correlation functional; DFT, density-functional theory; EXAFS, extended X-ray absorption fine structure; IEFPCM, integral equation formalism for the polarizable continuum model; INT, intermediate; IPN, isopenicillin N; IPNS, isopenicillin N synthase; ONIOM, our own N-layered integrated molecular orbital + molecular mechanics; QM/MM, quantum mechanics/molecular mechanics; TST, transition-state theory; TS, transition state; 4-HPPD, 4-hydroxyphenylpyruvate dioxygenase.

10.1021/bi701577q CCC: $40.75
Published on Web 12/29/2007

Scheme 1: Enzymatic Reaction Catalyzed by Isopenicillin N Synthase (IPNS)

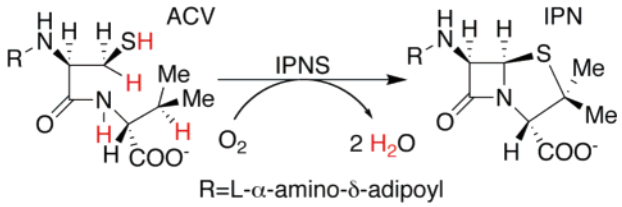

site (*16*) or by tuning the Fe(II)/Fe(III) redox potential. No O_2-bound state has yet been experimentally observed; instead, a NO-bound analogue serves as a model compound (*11*, *12*, *22*). NO binds in a position trans to Asp216, and it is assumed that O_2 binds in the same position (see Scheme 2).

Kinetic isotope effects (*23*) and the crystallographic observation of a monocyclic β-lactam ring in the substrate analogue ACmC (*13*) suggest that formation of the four-membered β-lactam ring is completed before formation of the C−S bond in the five-membered thiazolidine ring. The iron-bound dioxygen species should therefore first activate the cysteine β-C−H bond, leading to a ferrous peroxide [Fe(II)−OOH]. According to the proposal in ref *4*, the peroxide should then abstract the valine N−H proton to generate a ferryl−oxo [Fe(IV)═O] species and a water molecule. Concerted with ferryl−oxo formation, the valine nitrogen performs a nucleophilic attack on the cysteine β-carbon, which leads to cyclization of the β-lactam ring.

Generation of a high-valent ferryl−oxo species is a common theme, shared by many non-heme iron enzymes. This intermediate is often formed by oxidation of a cofactor like α-keto acid or tetrahydrobiopterin (*6*), but in IPNS, it is generated by the two-electron oxidative cyclization of the substrate. There is little doubt that a ferryl−oxo intermediate is formed in IPNS, but a previous study using density-functional theory (DFT) disfavored parts of the mechanism proposed in ref *4*, because the barrier for O−O bond cleavage was prohibitively high (*24*). An alternative mechanism was suggested instead, but a re-examination of the results from ref *24* raised some questions regarding this alternative proposal.

After β-lactam ring formation, the enzymatic mechanism seems straightforward. The high-valent ferryl−oxo species is a powerful oxidant and can be used in a variety of reactions, e.g., oxygenations, hydroperoxidations, and epoxidations. In IPNS, it should activate the C−H bond of the tertiary valine β-carbon. This creates a carbon-centered substrate radical and a ferric−hydroxy [Fe(III)−OH] species. Independent deuterium kinetic isotope effects for both the cysteine β-carbon and the valine β-carbon suggest that both C−H bond activation steps are at least partially rate-limiting (*25*).

The aliphatic carbon radical then attacks the cysteine thiolate to close the thiazolidine ring and complete the formation of isopenicillin N (see Scheme 2). An alternative reaction, observed in other many enzymes that form ferryl−oxo intermediates, is hydroxylation of the substrate in an oxygen rebound mechanism (*6*). The reason why IPNS preferentially catalyzes ring formation rather than hydroxylation still remains to be explained.

This reinvestigation of the catalytic mechanism in IPNS using density-functional modeling was prompted by the new information available from experimental (*7*) and theoretical (*26*, *27*) studies recently performed on other members of the 2-histidine-1-carboxylate enzyme family. The purpose of this study is to find a mechanism for O−O bond heterolysis, consistent with the experimentally estimated reaction barrier of 16.8 kcal/mol (*28*). The expected accuracy of density-functional calculations for transition metal enzymes is in the 5 kcal/mol range. This level of accuracy makes it difficult to calculate and compare exact rates of individual steps, but the method is in general sufficiently accurate to discriminate between different mechanistic proposals for the same reaction.

COMPUTATIONAL METHODS

All calculations were performed on an active-site model of the iron center. The model includes Fe, the side chains of the amino acids coordinating iron (His214, Asp216, and His270), the water ligand (WAT398) (*4*), and the cysteine-valine part of the substrate where the chemical transformation occurs (see Figure 1). Only the first-shell amino acids have been included, partly because they are the only ones known to be essential for catalysis (*18*). Histidine is modeled as 4-methylimidazole, and aspartate is modeled as acetate. The initial model system (model A) consists of 65 atoms.

Initial coordinates are taken from X-ray structure 1BLZ (1.45 Å resolution), which represents the ACV−Fe(II)−NO state, and NO is replaced by O_2. To avoid artificial changes in geometry caused by an incomplete hydrogen bond network in the truncated model, Cartesian coordinates of selected atoms were kept frozen during optimizations (see Figure 1). However, during the reaction, the substrate goes from a linear molecule to a bicyclic one, and the coordinates of the substrate can therefore not be kept frozen in the same position during the entire reaction. To minimize problems with artificial hydrogen bonds, two changes are made to the model during the reaction. Starting from the full model described above (model A), model B excludes the carboxylate group before the closing of the β-lactam ring, while model C also excludes the water molecule formed after O−O bond heterolysis (see Figure 1). Model A has a net charge of −1, while models B and C are neutral.

Calculations were performed using Gaussian03 (*29*). Geometries were optimized using the hybrid functional B3LYP (*30*) and the 6-31G(d) basis set. Final energies were evaluated using the 6-311+G(d,p) basis set. Hybrid density functional is the only method that can treat systems of this size with reasonable accuracy. The popular B3LYP functional has been shown to perform relatively well for a large number of different transition metal applications (*31*), but errors in the 5 kcal/mol range have to be expected.

All calculations were performed using the unrestricted formalism. Selected stationary points were calculated with different spin multiplicities (septet, quintet, and triplet). On the basis of previous results from enzymes with similar active sites, the singlet state is assumed to be unstable (*26*). For the reactant (Fe−O_2 side-on), the singlet state is unstable by approximately 20 kcal/mol. Open-shell species with antiferromagnetic coupling have not been corrected for spin contamination. For the quintet Fe−O_2 species (end-on binding), the correction using the Heisenberg Hamiltonian formalism (*32*) would have been 0.7 kcal/mol, and for the

Scheme 2: Proposed Scheme for the Substrate Reaction in Isopenicillin N Synthase, Adapted from ref *4*[a]

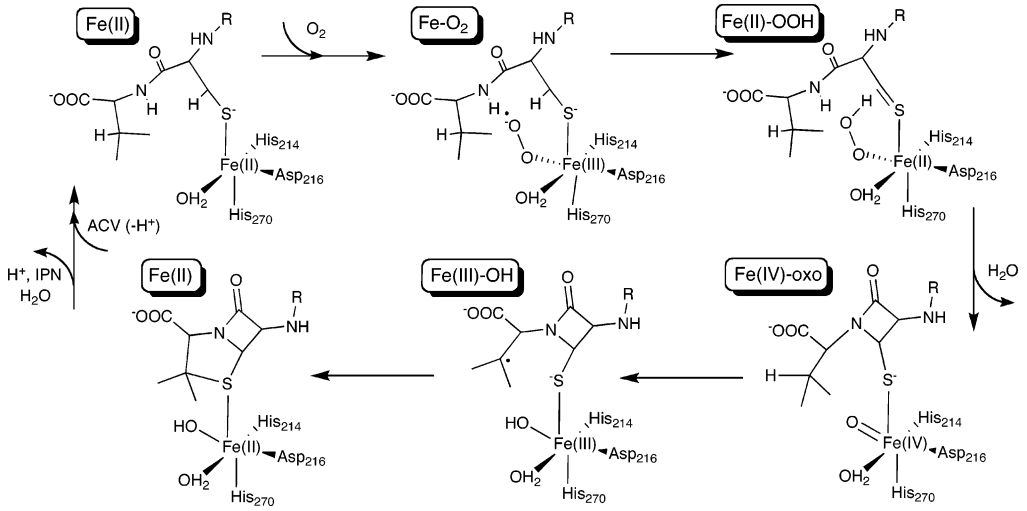

[a] Binding of oxygen initiates formation of the four-membered β-lactam ring, followed by formation of the five-membered thiazolidine ring.

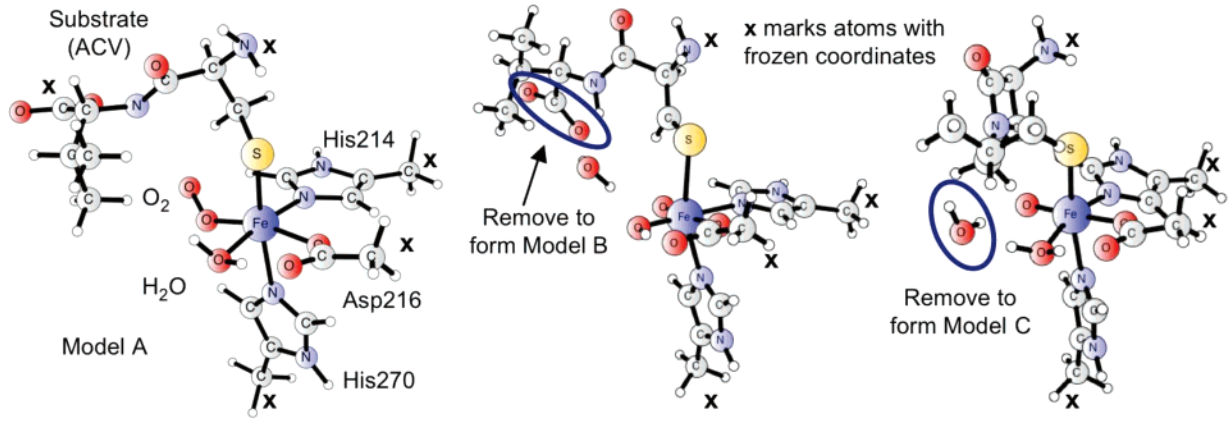

FIGURE 1: Active-site models used in this study. Atoms whose Cartesian coordinates have been frozen at the X-ray structure are marked with an x. Model A is used for stationary points **1**−**9**. Model B is used for stationary points **9**−**13** and is derived from model A by removing the substrate carboxylate. Model C is used for stationary points **13**−**18** and is obtained after removing the water molecule, formed during O−O bond cleavage, from model B.

quintet intermediate **16** [Fe(III)−OH with a substrate radical], it would have been <0.2 kcal/mol. For intermediate **16**, calculations on alternative spin states have been performed with a model without methyl groups on the amino acid models.

Electronic energies were corrected by adding zero-point, thermal, and solvent contributions. These effects were evaluated using the same basis set as in the optimization [6-31G(d)]. Zero-point energy and thermal corrections were taken from unscaled frequencies of a fully optimized model without methyl groups on the amino acid models. Zero-point corrections are important for the C−H bond activation steps because they lower the barriers of these steps by 3−5 kcal/mol. Solvent corrections were calculated using IEFPCM (*33*) with a dielectric constant of 4, mimicking the interior of a protein. In these calculations, the solvent effects are particularly large for intermediate **5** (7 kcal/mol). This large effect indicates a slightly unbalanced computational model. The main problem is the substrate carboxylate that has no hydrogen bonding interactions in the reactant but is involved in hydrogen binding with a peroxide species in intermediate **5**. Fortunately, the calculated rate-limiting barriers do not depend on the energy of this intermediate.

All reported energies represent an estimate of ΔG or $\Delta G^{\ddagger}$ for each stationary point. Comparisons with the experimentally determined rate are made by using the standard form of transition-state theory (TST). In TST, a rate of 3.2 s^{-1} corresponds to a barrier of 16.8 kcal/mol (*28*).

RESULTS AND DISCUSSION

The modeled mechanism for formation of isopenicillin N involves a large number of stationary points. To facilitate the discussion, stationary points are assigned numbers (appearing in boldface) on the basis of the order in which they appear along the reaction coordinate. When necessary, the nature of the stationary point is indicated by a label, TS for transition state and INT for a reaction intermediate. For some steps, e.g., bond rotations, transition states have not been optimized and two intermediates may therefore follow directly after each other in the potential energy diagram. Structures that are stationary states on the B3LYP/6-31G(d) surface used for optimization, but not after the energy has been corrected for basis set, zero-point, thermal, and solvent effects, are labeled "TS" and "INT", respectively. For the most stationary points, only the quintet state has been modeled. States with septet and triplet

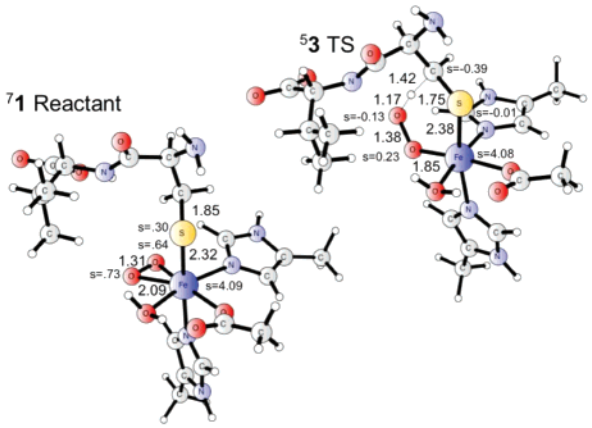

FIGURE 2: Reactant and transition state for Cys-β-C−H activation by a ferric−superoxo [Fe(III)−OO$^-$] species. Labels show selected bond distances (in angstroms) and Mulliken spin populations.

multiplicities are indicated with a left superscript, e.g., ^{7}**1** and ^{3}**1**, respectively.

Cys-β-C−H Activation. This investigation includes all the steps involved in the chemical transformation of the substrate, with the exception of the substrate binding step. An important potential consequence of substrate binding is deprotonation of the thiol group upon ligation to iron. It is difficult to calculate protonation states in proteins using active-site models, but for the substrate, the protonation state can be assigned from indirect observations. For the Fe(II)−ACV complex, EXAFS gives an Fe−S distance of ∼2.35 Å (*10*, *11*), and this can be reproduced only with a deprotonated substrate (Fe−S distance of 2.32 Å). Models with protonated thiols give Fe−S distances of >2.50 Å. The acceptor of the thiol proton is assumed to be outside the active-site model.

The O_2 molecule enters the active site after substrate binding. Using the active-site model presented here, O_2 binding was previously found to be endergonic by 10.6 kcal/mol (*34*). A high endergonicity for this step is in line with previous experience from active-site models (*26*, *35*, *36*) but seems to be in contradiction with the observed reactivity of these enzymes. ONIOM QM/MM calculations were therefore performed on the O_2 binding step in IPNS, and the results confirm that binding of dioxygen is not accurately handled by active-site models. Including the protein environment stabilizes O_2 binding by 8−10 kcal/mol and gives an almost thermoneutral reaction, as reported by us previously (*34*). In this investigation, the dioxygen-bound state is therefore taken as the reference state.

Throughout this study, assignments of electronic structures and oxidation states are made on the basis of bond distances and Mulliken spin populations. In the reactant (^{7}**1** in Figure 2), iron has a spin population of 4.09. This corresponds to a high-spin ^{6}Fe(III) state, although ^{6}Fe(III) formally has five unpaired electrons in the 3d orbitals. Using essentially the same methods as in this study, spin populations of 3.7−3.8 approximately correspond to ^{5}Fe(II), 4.0−4.2 to ^{6}Fe(III), and 3.0−3.3 to ^{5}Fe(IV) (*37*). The difference between the calculated spin populations and the formal number of unpaired d-electrons is due to backdonation from ligand β-orbitals. Consequently, spin formally assigned to d-orbitals on Fe is delocalized to all the ligands. However, the amount of delocalization is almost the same for all iron complexes of the same oxidation state, and spin populations are therefore

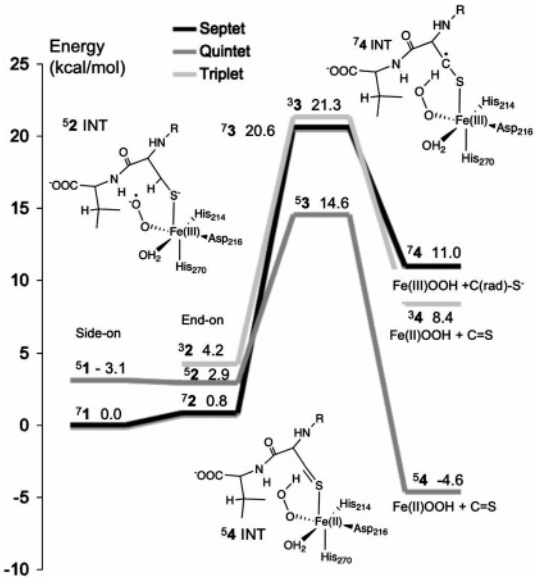

FIGURE 3: Calculated potential energy diagram for Cys-β-C−H bond activation on septet, quintet, and triplet surfaces. Boldface numbers refer to the order of the stationary state, starting from **1** (Fe−O_2 side-on reactant). Lightface numbers represent relative energies in kilocalories per mole. The minimum of the seam of crossing between septet and quintet surfaces has not been calculated, but the energy should be located close to ^{5}**2**.

good indicators of the oxidation states of high-spin iron systems. In the B3LYP description, the reactant (^{7}**1**) is thus a ferric−superoxo species [Fe(III)−OO$^-$] obtained by transfer of one electron from Fe(II) to an antibonding 3π-orbital in O_2. This assignment is consistent with the detailed orbital analysis in ref *22*.

The most stable O_2-bound state is a septet with side-on coordination (both oxygen atoms coordinate to iron) (^{7}**1**), and this is taken as the reference (zero) of energy. The relative energy of the most stable quintet state (^{5}**2** with end-on coordination having one coordinating oxygen) is 2.9 kcal/mol (see Figure 3). With this accuracy, this energy difference is too small to allow a definite assignment of the spin state in the enzyme. Both these states are assigned as ferric−superoxo states, and the major difference is the alignment in the spin on the superoxo radical (parallel or antiparallel to the spins on iron). A triplet state (^{3}**2**) also exists at 4.2 kcal/mol. This state has substantial Fe(II)−O_2 character with a slightly shorter O−O bond (see ref *34* for details).

Binding of dioxygen to the high-spin iron center removes the constraints of a formally spin-forbidden reaction between triplet oxygen and the closed-shell ACV substrate. According to Scheme 2, the next step is activation of the Cys-β-C−H bond. Brown et al. (*22*) have recently shown that the frontier molecular orbital of the Fe(III)−superoxide species, the O_2 π*-orbital, is oriented so that it forms a σ-overlap with the hydrogen.

Proceeding from the stable reactant (^{7}**1**) on the septet surface, a transition state (^{7}**3**) is reached at 20.6 kcal/mol. This leads to a high-spin ferric−peroxide intermediate [Fe(III)−OOH] and a substrate radical centered on the β-carbon (^{7}**4** INT at 11.0 kcal/mol). To reach a septet state, the spin on the substrate radical is necessarily aligned in parallel with the spins of the five d-electrons in Fe(III).

Although the quintet state is not the stable reactant, the reaction on the quintet surface turns out to be more favorable

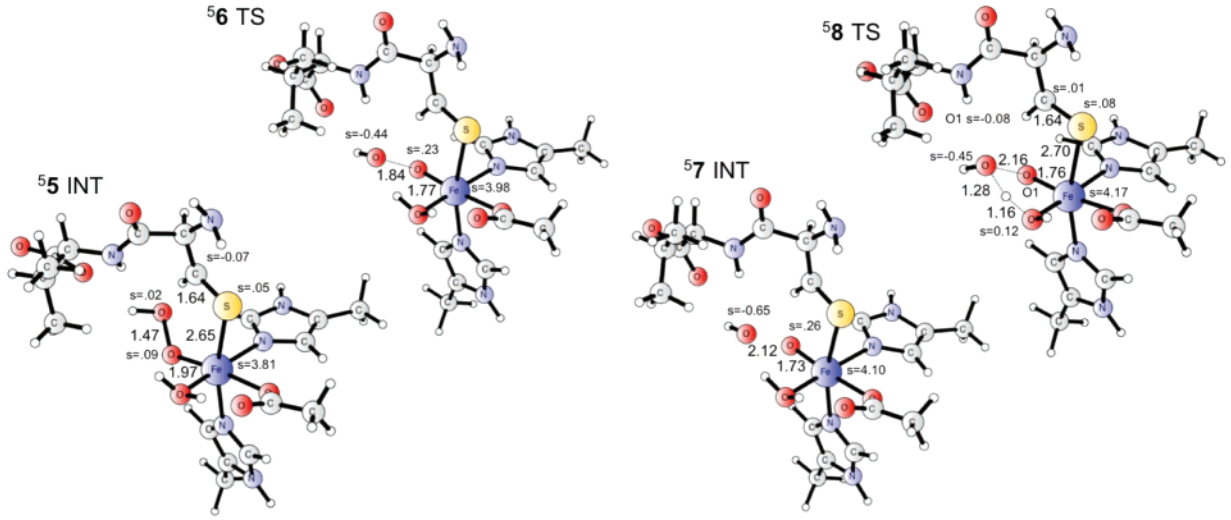

FIGURE 4: Reactant, transition states, and intermediate for cleavage of the O−O bond in the Fe(II)−OOH intermediate leading to formation of an Fe(IV)−oxo species. Labels give selected bond distances (in angstroms) and important Mulliken spin populations.

because it leads to a more stable product. On the quintet surface, the barrier for Cys-β-C−H bond activation (^{5}**3** TS) is at 14.6 kcal/mol, significantly lower than on the septet surface. This step should be at least partially rate-limiting, and compared to the experimental barrier of 16.8 kcal/mol, the calculated barrier presented here is slightly underestimated.

Because the reaction occurs on the quintet surface, a transition between the septet and the quintet surfaces must occur. The most stable conformation on the quintet surface is end-on binding of dioxygen (^{5}**2** INT) (see ref *34* for details). Previous calculations on similar active sites showed that the minimum-energy crossing point between the septet and quintet was located <1 kcal/mol above the quintet structure (*26*). Together with strong spin-orbit coupling in the transition-metal system, the spin transition should therefore be very fast and not affect the rate of the reaction.

The resulting quintet intermediate (^{5}**4** INT) is relatively stable [−4.6 kcal/mol (see Figure 3)]. A rotation of the FeO−OH bond results in an even lower energy (−10.8 kcal/mol) due to formation of better hydrogen bonds with the carboxylate group of the substrate (^{5}**5** INT shown in Figure 4). In the real protein, the carboxylate is included in a hydrogen bonding network with residues Tyr189, Arg279 (through a water molecule), and Ser281. When these additional residues are included in the QM model, the hydrogen bond between substrate and peroxide does not develop. In the new model, the relative energy of intermediate ^{5}**5** INT increases by approximately 3 kcal/mol. Fortunately, the barrier for the proceeding transition state (^{5}**6** TS) changes by less than 1 kcal/mol. Since these corrections do not affect the conclusions of this paper, they have not been included in the results.

If we look more closely at the electronic structure of the intermediate ^{5}**4**, it is clear that it corresponds to a ferrous−peroxide intermediate [Fe(II)−OOH] and a double bond between carbon and sulfur. This assignment can be derived from the low spin density on the cysteine β-carbon (−0.07), the spin population on iron (3.81), the shorter C−S distance (1.64 Å compared to 1.85 Å in the reactant), and the longer S−Fe distance (2.65 Å compared to 2.32 Å in the reactant); see Figure 4 for details.

The very large difference in stability between the septet (^{7}**4**) and quintet (^{5}**4**) intermediates can be explained by an additional transfer of an electron from the substrate to iron. This electron transfer can take place only in the quintet state, because the unpaired substrate electron must be transferred to an empty β-orbital on Fe(III). Activation of the Cys-β-C−H bond thus leads to abstraction of one proton and two electrons from the substrate. This may not seem consistent with the reaction described by transition state ^{5}**3**, since it has all the characteristics of a hydrogen atom transfer, with significant spin (0.39) developing on the carbon atom (see Figure 2). Following the intrinsic reaction coordinate (IRC) from ^{5}**3** TS further increases the spin on carbon to a maximum of 0.65, but this substrate radical is not an intermediate in these calculations. Instead, the second electron is transferred from the substrate, and the system relaxes to the Fe(II)−OOH intermediate without any barrier.

The corresponding intermediate on the triplet surface ^{3}**4** also represents an Fe(II)−OOH state, but it is significantly higher in energy (by 13 kcal/mol) than the quintet state, since it requires intermediate spin on iron Fe(II).

There appears to be a relatively straightforward reason why Cys-β-C−H bond activation, and therefore β-lactam ring formation, occurs prior to Val-β-C−H bond activation. If we look at the substrate model only, the strength of the Cys-β-C−H bond is significantly lower (by 11 kcal/mol) than that of the Val-β-C−H bond. Carbon-centered radicals are stabilized in dialkyl sulfides (*38*), and the presence of the thiolate should therefore make the C−H bond weaker. The transfer of the second substrate electron to iron also helps to stabilize transition state ^{5}**3**. The Cys-β-C−H bond can therefore be activated by the comparably weaker Fe(III)−OO^- oxidant, while the corresponding bond of the valine β-carbon can be activated only by the strong Fe(IV)═O oxidant, formed after O−O bond heterolysis.

The description of the C−H bond activation step in this study is different from that of the previous DFT study by Wirstam et al. (*24*). In that study, the mechanism proposed here was not supported because the barrier for C−H bond activation was only 1.1 kcal/mol, which is not consistent with kinetic isotope experiments showing that this step is partially

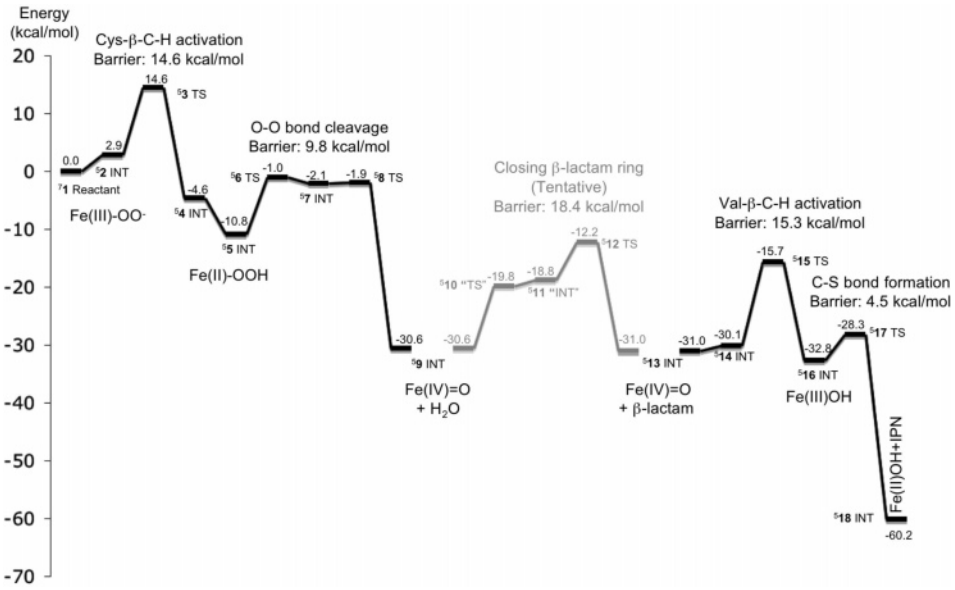

FIGURE 5: Calculated potential energy diagram for the enzymatic reaction catalyzed by isopenicillin N synthase. Stationary states are labeled with boldface numbers in sequential order. Lightface numbers are relative energies compared to that of ^{7}**1** (Fe−O_2 reactant) in kilocalories per mole. Intermediate ^{5}**9** is calculated using both model A and model B, while intermediate ^{5}**13** is calculated using models B and C.

rate limiting (*23*). A possible explanation of the results in ref *24* is that the low barrier is caused by an unstable electronic configuration in the reactant. Reactant ^{7}**1** is an Fe(III)−OO^- state, similar to the ones obtained for other oxygen-activated non-heme enzymes (*26*), while the reactant in ref *24* is an Fe(II) state with significant spin on the substrate thiolate but very low spin density on oxygen. In this investigation, that state could not be reproduced, even when the same model was used. However, if the transition state and resulting intermediate represent the same states in the two studies (they have similar spin populations), the Fe(III)−OO^- reactant (^{7}**1**) is approximately 10 kcal/mol more stable than the reactant used in ref *24*.

The study by Wirstam et al. instead preferred a reaction in which the Fe−O_2 species accepts a proton from an external donor before the C−H bond is activated. This leads to an acceptable barrier for O−O bond cleavage in a reaction with Cys-β-C−H. However, in this study, the O_2 species has a lower proton affinity than the substrate thiolate (by 15 kcal/mol in ^{7}**1**). Since EXAFS data suggest that there is no proton on the thiolate (see the discussion above), dioxygen should therefore not be protonated either. If the minimum energy penalty for protonating O_2 is 15 kcal/mol, the transition state for O−O bond cleavage in ref *24* becomes too high (30 kcal/mol).

O−O Bond Cleavage and β*-Lactam Ring Formation.* After generation of the peroxide intermediate, a seemingly attractive mechanism is abstraction of the valine N−H proton by the peroxide to generate a ferryl−oxo [Fe(IV)═O] species and a water molecule. At the same time, the valine nitrogen should perform a nucleophilic attack on the cysteine β-carbon, which leads to formation of the β-lactam ring (see Scheme 2). However, as mentioned in the introductory section, one of the main conclusions from the previous DFT study of isopenicillin N synthase was that this mechanism had an exceedingly high barrier (*24*). This study supports that observation. Cleaving the O−O bond by protonation from the valine N−H group has a barrier of 30.9 kcal/mol and occurs after the C−N bond in the β-lactam ring is almost formed (C−N distance of 1.62 Å). Although the two models are slightly different, this transition state is very similar to the one optimized in ref *24*. With this model, all other tested combinations of concerted and stepwise reactions involving these three bonds gave similar or higher barriers.

In a search for an alternative mechanism, it was noted that formation of a ferryl−oxo intermediate is a common step for many mononuclear non-heme enzymes. A number of these reactions have also been modeled theoretically (see, for example, ref *27*), and ideas for alternative mechanisms were therefore sought among this enzyme family. In several enzymes, formation of an Fe(IV)═O intermediate from an Fe(II)−OOR species generates a negative charge on one of the other iron ligands. In α-keto acid-dependent dioxygenases, a carbonyl becomes the anionic part of a carboxylic acid, while in pterin-dependent hydroxylases, O−O bond cleavage leads to formation of a HO−Fe(IV)═O species (*26*). More specifically, in pterin-dependent hydroxylases, O−O bond heterolysis is assisted by a ligating water molecule that donates a proton to the distal oxygen and thereby generates the HO−Fe(IV)═O intermediate.

IPNS also has a water ligand bound to iron, and abstracting a proton from this water leads to O−O bond cleavage with a barrier of 9.8 kcal/mol. The calculated potential energy diagram for the full isopenicillin N reaction, including O−O bond cleavage, is shown in Figure 5. The initial reaction coordinate, starting from the Fe(II)−OOH intermediate ^{5}**5**, describes homolytic O−O bond cleavage with a transfer of a single electron from iron to an antibonding O−O σ*-orbital. The transition state (^{5}**6** TS in Figure 4) involves only O−O bond breaking (bond distance of 1.84 Å) and leads to a shallow minimum (^{5}**7** INT) which is essentially Fe(III) (Mulliken spin of 4.10) antiferromagnetically coupled to a hydroxyl radical (Mulliken spin of −0.65). From this metastable intermediate, a proton is transferred from the iron-bound water ligand, coupled to a second electron transfer from iron, via ^{5}**8** TS (in Figure 4). The total O−O bond

Scheme 3: Similar Reaction Mechanisms for O−O Bond Cleavage in Three Non-Heme Iron Enzymes; IPNS (present study), a Pterin-Dependent Hydroxylase (*35*), and the α-Keto Acid-Dependent Clavaminate Synthase (CAS) (*40*)[a]

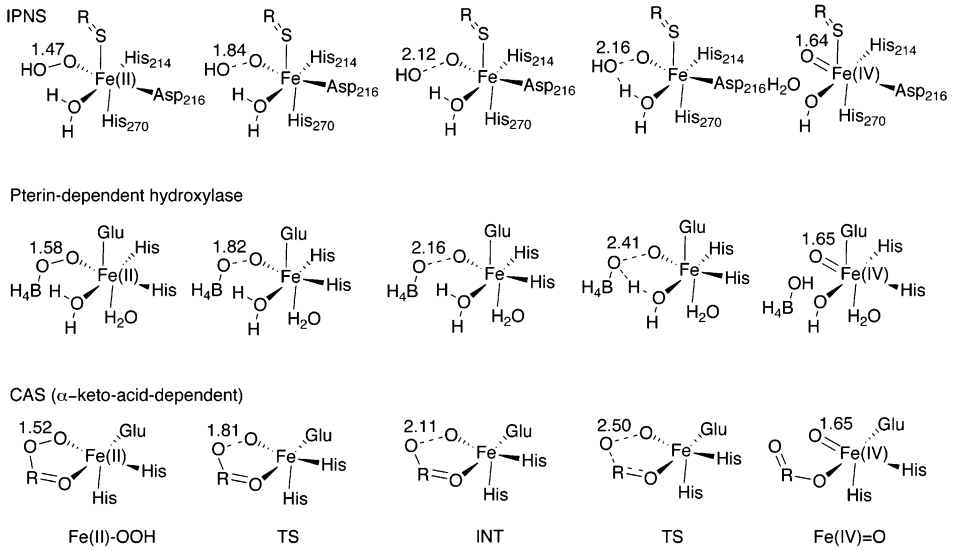

[a] Numbers represent O−O bond distances in angstroms, except for the Fe(IV)═O state where the label shows the iron−oxo distance.

cleavage reaction is therefore heterolytic and leads to formation of a water molecule and a HO−Fe(IV)═O intermediate (^{5}**9**). The reaction is highly exothermic (see Figure 5).

The pathway for O−O bond cleavage looks highly similar to modeled reactions for pterin-dependent hydroxylases (*35*), a biomimetic non-heme iron complex (*39*), and the α-keto acid-dependent clavaminate synthase (*40*) (see Scheme 3). All of them show an initial O−O bond elongation, coupled to a single-electron transfer, followed by a second electron transfer leading to the Fe(IV)═O species. For all modeled reactions, the O−O bond distances for the intermediate as well as for the first transition state are very similar, while the O−O bond distance for the second transition state seems to depend on the exothermicity of the reaction (shorter bond lengths for more exothermal reactions). Whether the intermediate appears on the calculated potential energy surface seems to be determined by minor details; i.e., the modeled reaction is stepwise for clavaminate synthase but not in 4-HPPD (*41*), despite both of them performing the same reaction, oxidative decarboxylation of the α-keto acid cofactor. For all practical purposes, O−O bond heterolysis can be considered as a concerted reaction.

Another common feature for the three enzymes shown in Scheme 3 is that O−O bond cleavage is not the rate-limiting step. Instead, the barrier for two-electron oxidation of the cofactor (or substrate in the case of IPNS) is consistently higher.

Despite the overall similarities, there are also differences among the three reactions in Scheme 3. Most noticeably, in the pterin-dependent hydroxylases and clavaminate synthase the O_2 group initially binds in a position trans to a histidine ligand while in IPNS it binds trans to the carboxylate. Another difference is that the clavaminate synthase active site is modeled as five-coordinate after release of CO_2 in the preceding reaction, while the other models are six-coordinate. The barrier for O−O bond cleavage is higher in IPNS than in the pterin-dependent hydroxylase and clavaminate synthase (9.8 kcal/mol compared to 4.8 and 4.7 kcal/mol, respectively).

The high barrier for O−O bond cleavage by protonation from the valine N−H group (the mechanism proposed in ref *4*) is slightly puzzling. After accepting two electrons from the substrate but only one proton, the Fe−OOH species has a high proton affinity, and it is not clear why the Val-N−H species is not a suitable proton donor. Closing the *β*-lactam ring breaks the C═S bond and regenerates the negative thiolate iron ligand. This reaction thus also creates a new negative iron ligand. Despite this, the presently modeled barrier is very high. Although a number of different reaction pathways have been explored, this pathway should not be completely ruled out until a convincing explanation for the high barrier can be found. A possible explanation would be that as long as the C−N bond of the *β*-lactam ring has not yet formed, Val-N−H is a worse proton donor than water bound to iron. Protonation from Val-N−H in intermediate ^{5}**7** therefore requires simultaneous O−O bond cleavage and C−N bond formation. However, these reactions are not strongly coupled in these calculations, and the barriers for the two separate reactions seem to be added.

In the Fe(IV)═O intermediate (^{5}**9** INT in Figure 6), the spin on iron is 3.21 while substantial spin is located on the oxo group (Mulliken spin of 0.46). The Fe−O bond formally has double-bond character that originates from the distribution of eight electrons in five FeO orbitals (σ, π, π^*). Since the two π^*-orbitals are singly occupied, this causes significant spin to be assigned to oxygen. The identity of the Fe(IV)−oxo state is supported by the calculated Fe−O distance of 1.64 Å, which is similar to experimentally measured distances for Fe(IV)═O complexes (1.62 Å) (*42*, *43*). Experiments suggest that the high-spin complex is the most stable (*44*), and computationally, triplet (^{3}**9**) and septet (^{7}**9**) states are unstable by 5.2 and 10.3 kcal/mol, respectively. Because these states are unstable also in the Fe(II)−OOH state (^{5}**4** INT), O−O bond cleavage was not modeled for these spin states.

An alternative reaction pathway for O−O bond cleavage on the quintet potential energy surface can be explored by decreasing the O−O bond distance from the Fe(IV)═O intermediate (^{5}**9**). At an O−O distance of 2.0 Å, the energy

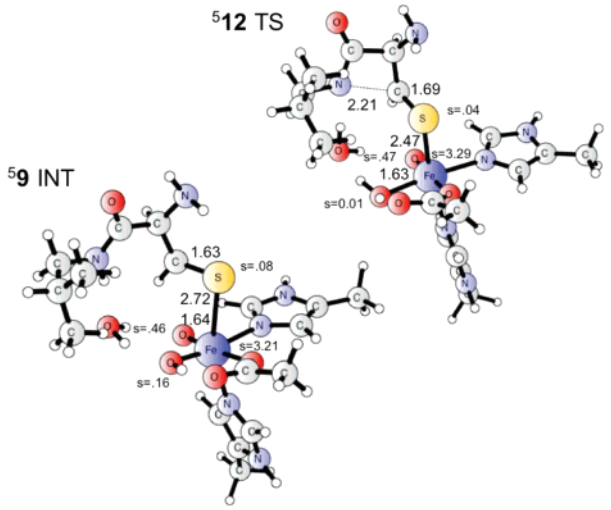

FIGURE 6: Reactant and tentative transition state for closing of the β-lactam ring after formation of an Fe(IV)═O species. Labels give selected bond distances (in angstroms) and important Mulliken spin populations.

is lower than for the reaction path outlined above; however, the electronic configuration still represents an Fe(IV)═O state, and the proton resides on the water molecule. Decreasing the O−O bond distance further increases the energy for this configuration, and no low-lying transition state could be found.

The O−O bond heterolysis reaction modeled here occurs without direct involvement of the substrate in the bond cleavage step. However, the substrate has already played a critical role because it contributed the two electrons required for formation of the Fe(IV)═O intermediate already in the first reaction step (^{7}**1** → ^{5}**4**). The ACV substrate has at this stage thus already performed the same role as the α-keto acid and tetrahydrobiopterin cofactors perform in other non-heme enzymes.

To finally close the β-lactam ring, the substrate should lose the valine N−H proton and form a bond between the cysteine β-carbon and the valine nitrogen. Formation of the C−N bond re-creates the negative thiolate ligand, a process that is likely to increase the proton affinity of the water-derived iron ligand and lead to its protonation. From a modeling perspective, this is a complicated reaction that requires an accurate description of the correct acceptor of the N−H proton, the proton-transfer pathway to the hydroxo ligand, and the changes in hydrogen bond patterns that occur during the reaction. This model is too limited to take all these factors into account. However, to illustrate that the barrier is not prohibitively high, a mechanism for ring closure has still been calculated. Neither the barrier nor the exact reaction mechanism should probably be taken literally, and because of the tentative nature of this mechanism, it will be only briefly described.

The assumption that the Fe−OH ligand directly accepts the Val-N−H proton is reasonable and enables a potential energy profile to be constructed without use of any external parameters, i.e., proton affinities of the surrounding media. In the modeling, the newly formed water molecule acts as a proton shuttle between the substrate and the hydroxo group. The substrate carboxylate is removed from the model to prevent the formation of artificial hydrogen bonds (model B).

On the uncorrected surface, closing of the β-lactam ring proceeds through several stationary points but after all corrections have been added, only one transition state remains (^{5}**12** TS in Figure 6). The presence of a single transition state shows that ring closure is a concerted reaction with transfer of a proton from the valine N−H group to the Fe−OH ligand occurring simultaneously with C−N bond formation. Although the optimized transition structure (^{5}**12** TS) shows that proton transfer has been completed at an early stage of the reaction, this can be an artifact from the optimization on the uncorrected potential energy surface.

The calculated barrier for formation of β-lactam through ^{5}**12** TS is relatively high, 18.4 kcal/mol. This barrier is close to the experimental limit of 16.8 kcal/mol and could represent another rate-limiting step of the IPNS reaction. The common interpretation is that IPNS has two rate-limiting steps, activation of the valine and the cysteine β-C−H bonds, but the proposed mechanism does not contradict the available experimental data.

First, this accuracy allows only a determination of relative energies with an accuracy of 3−5 kcal/mol. In addition, this mechanism is tentative and lower barriers could exist for other proton transfer pathways. The exact height of the barrier must therefore be treated with considerable caution. If the barrier is 3−5 kcal/mol lower (i.e., 13−15 kcal/mol), it will be kinetically silent compared to the C−H activation steps where the barriers experimentally are known to be around 17 kcal/mol.

Second, the suggestion of two rate-limiting steps is based on kinetic isotope experiments that show independent effects for both cysteine β-C−H and valine β-C−H protons (*23*). Although these experiments clearly show that no other reaction step can have a higher barrier, the results do not exclude a third reaction step with a marginally lower barrier. Deuterium substitution increases the barriers of the C−H bond activation steps, and the kinetic effect of a potential third step would largely disappear.

A signature of a third rate-limiting step would be if isotope effects could be observed for the valine-N−H proton. Unfortunately, the lack of an effect is not conclusive. It could mean either that the barrier for β-lactam ring formation is much lower than what is presently modeled or that the ring closure transition state is dominated by formation of the C−N bond (as in ^{5}**12** TS).

In total, formation of the monocyclic β-lactam form of the substrate (^{5}**13** INT) from the open form (^{5}**9** INT) is slightly exothermal (see Figure 5). The open form should therefore not be observed under equilibrium conditions but could possibly be detected as a metastable intermediate. Crystallographic studies of the substrate analogue AcMC, which cannot undergo the second ring formation step, show that the closed β-lactam ring (*13*) is indeed the stable form of this intermediate.

Despite the Fe center not being redox active during the reaction, β-lactam ring formation probably does not occur before generation of the Fe(IV)═O species (i.e., from intermediate ^{5}**5**). Ring closure regenerates the thiolate ligand since it breaks the C═S bond (see Scheme 2), and this reaction is more favored when the oxidation state of iron is Fe(IV) compared to Fe(II). The detailed reaction mechanism cannot be calculated with the model presented here, because there is no suitable acceptor for the valine N−H proton (in

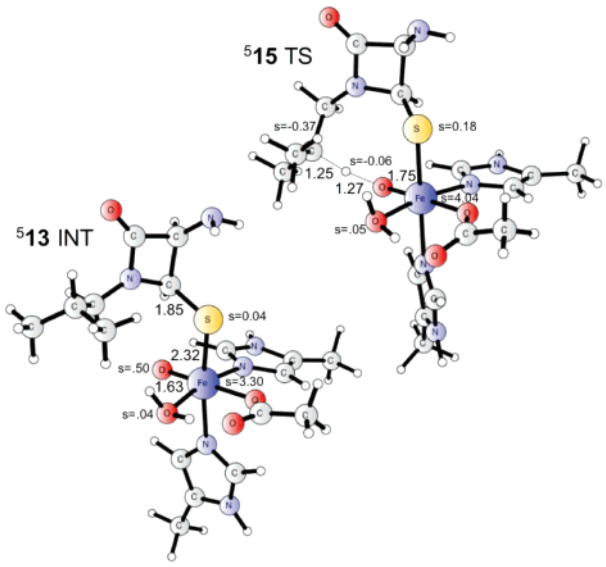

FIGURE 7: Reactant and transition state for valine β-C−H bond activation. Note that the isopropyl group needs to be rotated before it can be activated by the Fe(IV)═O intermediate. Labels give selected bond distances (in angstroms) and important Mulliken spin populations.

intermediate ^{5}**5**, the iron ligand is still water, not a hydroxo group). However, the energy required to shorten the C−N bond without proton transfer is significantly lower in ^{5}**9** INT [Fe(IV)] than in ^{5}**5** INT [Fe(II)].

*Val-**β**-C−H Activation and Thiazolidine Ring Formation.* The final stage of the reaction is activation of the C−H bond of the valine isopropyl group by the Fe(IV)−oxo intermediate, followed by formation of the second substrate ring. The modeled reaction supports the mechanistic proposal in Scheme 2. The reaction is complicated by the fact that in the X-ray structure, the Val-β-C−H bond actually points away from the iron center. A possibility is that the valine isopropyl group rotates during formation of the β-lactam ring, but in the model presented here, this did not occur (see ^{5}**13** INT in Figure 7). In an active-site model, the isopropyl group can be easily rotated so that the C−H bond faces the iron center (^{5}**14** INT). The Fe(IV)−oxo group then abstracts a hydrogen from the valine isopropyl group with a total barrier of 15.3 kcal/mol (see ^{5}**15** TS in Figures 5 and 7). In this step, the high-spin Fe(IV)═O complex is transformed into a high-spin Fe(III)−OH species, while the unpaired electron of the aliphatic radical has its spin aligned opposite to the spins on the ferric iron. The calculated barrier of 15.3 kcal/mol is rather close to the value of 14.6 kcal/mol calculated for the other rate-limiting step, activation of the cysteine β-C−H bond (^{5}**3** TS).

The substrate radical is proposed to be a short-lived reaction intermediate (^{5}**16** INT in Figure 8). Compared to that of the most stable Fe(IV)═O state (^{5}**13** INT), the relative energy of this state is −1.8 kcal/mol (see Figure 5). The unpaired electron on carbon does not couple strongly with the electrons on iron, so for this intermediate, a close-lying septet state exists (^{7}**16**). However, the septet state is unstable both in the forward and in the backward directions and should therefore not participate in the reaction.

In the final step, the carbon radical attacks the thiolate coordinating to iron and forms a new C−S bond, thus closing the thiazolidine ring and completing the formation of the bicyclic isopenicillin N molecule. The barrier for this step is only 4.5 kcal/mol (see Figure 5). During the reaction, an electron is transferred from the substrate to iron, and judging by the spin populations, this electron transfer occurs in a concerted manner with C−S bond formation. The spin population on carbon changes from −0.90 in intermediate ^{5}**16** to −0.67 in transition state ^{5}**17** (see Figure 8).

The final product is a bicyclic substrate with both β-lactam and thiazolidine rings, weakly coordinated to an Fe(II) complex. In the active-site model presented here, the IPN product loses coordination to iron (Fe−S distance of 4.2 Å), which is not supported by X-ray data (Fe−S distance of 2.87 Å) (*13*). With a relatively weak coordination, the exaggerated mobility of the active-site model leads to formation of artificial hydrogen bonds that successfully compete with iron coordination. As a consequence, the exothermicity of the final step may therefore be slightly overestimated with the small basis set. Large basis and solvent corrections may instead favor the tighter bound structure, and for a given structure, it is difficult to know which effect will dominate. In any case, the relative energy of the product should be considered to be approximate.

The results for thiazolidine ring formation are very similar to those obtained in the previous DFT study (*24*). However, the increased model size, i.e., including the methyl groups close to the valine β-carbon, significantly stabilizes the carbon radical intermediate.

Protonation of the Fe(II)−OH group should generate the second water molecule. Because no external proton donor is included, this reaction step has not been modeled. The donor should be the same as, or similar to, the group that accepted the S−H substrate proton upon substrate binding. It is therefore noted that the proton affinity of the Fe(II)−OH group is similar to the proton affinity of the thiolate in the reactant complex. The protonation of the Fe−OH ligand to complete the formation of two water molecules from dioxygen should therefore be relatively straightforward.

Finally, an attempt was made to understand why IPNS performs oxidative cyclization instead of substrate hydroxylation (i.e., prefers the rebound of sulfur over the rebound of oxygen). If we start from the substrate radical intermediate ^{5}**16**, formation of the C−O bond occurs concerted with a transfer of an electron from substrate to iron (TS ^{5}**17H** in Figure 8**)**. The calculated barrier is 8.2 kcal/mol, i.e., 3.7 kcal/mol higher than the corresponding barrier for C−S bond formation (4.5 kcal/mol). Electronically, the two transition states look rather similar with a small amount of spin transferred from the substrate radical to the iron center (see Figure 8). However, hydroxylation requires a rotation of the hydroxo ligand away from its equilibrium position in intermediate ^{5}**16**, where the hydrogen points directly at the substrate carbon radical. This leads to an initial increase in energy. Another factor that computationally favors the cyclization reaction is the entropy. A possible explanation of the entropy effect is that hydroxylation anchors the substrate to the iron center at two points (thiolate and hydroxo group) while cyclization leads to a single weak iron−thiol ligation with higher substrate flexibility.

When the two products are compared, the hydroxylated substrate is actually more stable than the observed isopenicillin N product. This is counterintuitive, because the factors disfavoring the hydroxylation transition state should also

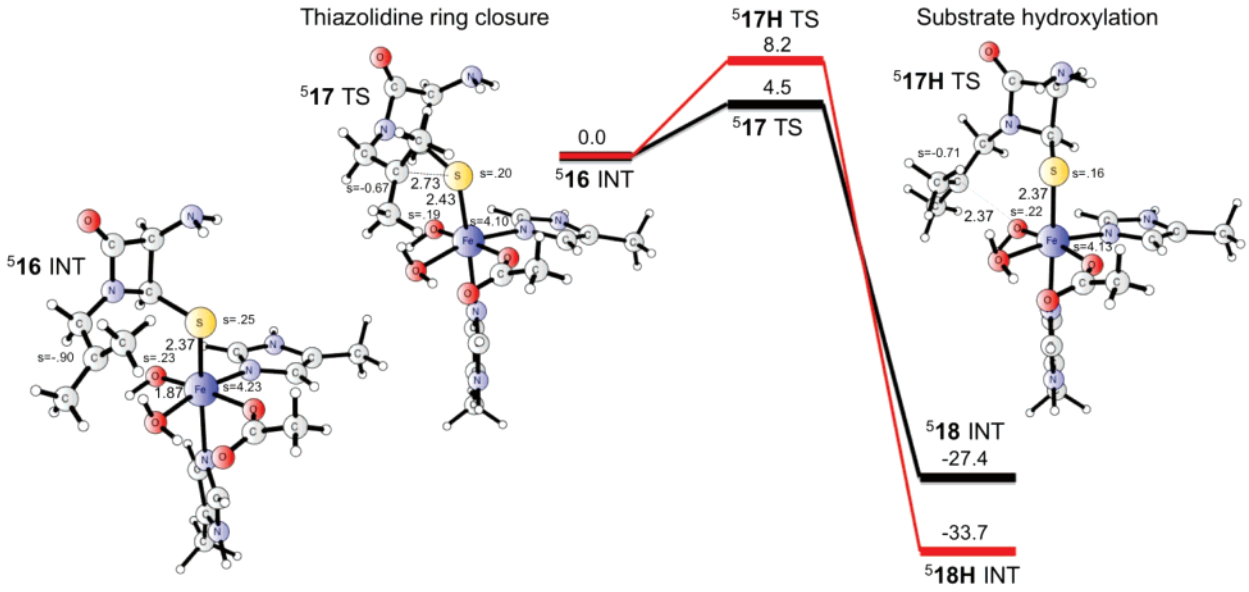

FIGURE 8: Reactant and transition states for formation of the thiazolidine ring (^{5}**17**) and for the competing substrate hydroxylation reaction (^{5}**17H**). Structure labels give selected bond distances (in angstroms) and important Mulliken spin populations. Relative energies compared to that of the common intermediate (^{5}**16**) are given in kilocalories per mole.

disfavor the hydroxylation product. However, the transition to a ferrous state leads to changes not directly connected to the transition state, i.e., relaxation of the iron coordination sphere that can favor the new orientation of the hydroxo group. It is also difficult to accurately calculate the relative energy of the two product states. As an example, the entropy calculation may break down for structures with very long and weak metal coordination bonds.

The calculations give the correct energetic ordering of the two transition states; i.e., hydroxylation is more than 100-fold slower than ring formation. The difference in barrier height can be the dominating factor in the determination of the selectivity of the final reaction step. Still, the energetic separation between the two rebound barriers is relatively small, and energy differences in the 3−5 kcal/mol range are at the accuracy limit of this computational method.

When it comes to the final reaction step, significant similarities between IPNS and the α-keto acid-dependent halogenases exist. Halogenases are believed to form a substrate radical through C−H bond activation, and the substrate then undergoes halogenation rather than hydroxylation. Recent results from density-functional modeling of a biomimetic complex that catalyzes substrate chlorination through a route similar to that of the halogenases show that the energetic barriers for the two competing reactions are too similar to explain the observed selectivity (*45*). More detailed calculations, e.g., including the full protein environment, may be required to fully understand the selectivity, both in the halogenases and in isopenicillin N synthase.

SUMMARY AND CONCLUSION

A potential energy surface has been constructed for the enzymatic transformation of ACV to isopenicillin N in IPNS. Three reaction steps show significant barriers (15−18 kcal/mol): activation of the cysteine *β*-C−H bond by an iron-bound superoxo radical, *β*-lactam ring formation, and activation of the valine *β*-C−H bond by a ferryl−oxo species. The C−H activation steps are known to be partially rate limiting, and the barriers agree very well with the experimental rate (corresponding to a barrier of 16.8 kcal/mol). The barrier for *β*-lactam ring formation (18.4 kcal/mol) is relatively high, but this can probably be explained by limitations in the model.

This study proposes a mechanism for O−O bond cleavage that is different from previous mechanistic proposals. O−O bond cleavage occurs with the help of an iron-ligating water molecule that donates a proton to the distal oxygen and generates the OH−Fe(IV)═O intermediate. The water ligand is regenerated upon closure of the *β*-lactam ring. This mechanism for O−O cleavage is almost identical to the reaction in pterin-dependent hydroxylases and very similar to the reaction in α-keto acid-dependent dioxygenases. Compared to a previous computational study using similar methods, the mechanism for Cys-*β*-C−H bond activation and *β*-lactam ring formation is different. The major differences come from a more stable electronic structure of a key intermediate, together with a new, previously untested mechanism for O−O bond cleavage.

The barrier for substrate hydroxylation, a reaction formally competing with thiazolidine ring closure, is calculated to be 4 kcal/mol higher than for ring closure. This difference in energy can be a dominating factor in determining the selectivity of the final reaction step.

The calculated potential energy profile can be used for further investigations of reactivity of modified substrates and enzyme mutants. However, such modeling requires a better understanding of interactions of the substrate with the protein while still accurately evaluating the reactivity of different substrate molecules. This objective can be achieved by the use of QM/MM models of the IPNS reaction, which is in progress in our laboratory.

ACKNOWLEDGMENT

The use of computational resources at the Fukui Institute for Fundamental Chemistry and at the Research Center of Computer Science (RCCS) at the Institute for Molecular Science (IMS) is acknowledged.

SUPPORTING INFORMATION AVAILABLE

List of stationary structures along the reaction pathway with energies (in hartrees) together with structure files (in XYZ format). This material is available free of charge via the Internet at http://pubs.acs.org.

REFERENCES

1. Schofield, C. J., Baldwin, J. E., Byford, M. F., Clifton, I., Hajdu, J., Hensgens, C., and Roach, P. (1997) Proteins of the penicillin biosynthesis pathway, *Curr. Opin. Struct. Biol. 7*, 857−864.
2. Baldwin, J. E., and Bradley, M. (1990) Isopenicillin N Synthase: Mechanistic Studies, *Chem. Rev. 90*, 1079−1088.
3. Schenk, W. A. (2000) Isopenicillin N synthase: An Enzyme at Work, *Angew. Chem., Int. Ed. 39*, 3409−3411.
4. Roach, P. L., Clifton, I. J., Hensgens, C. M. H., Shibata, N., Schofield, C. J., and Baldwin, J. E. (1997) Structure of isopenicillin N synthase complexed with substrate and the mechanism of penicillin, *Nature 387*, 827−830.
5. Andersson, I., Terwisscha van Scheltinga, A. C., and Valegård, K. (2001) Towards new β-lactam antibiotics, *Cell. Mol. Life Sci. 58*, 1897−1906.
6. Costas, M., Mehn, M. P., Jensen, M. P., and Que, L., Jr. (2004) Dioxygen Activation at Mononuclear Nonheme Iron Active Sites: Enzymes, Models, and Intermediates, *Chem. Rev. 104*, 939−986.
7. Koehntop, K. D., Emerson, J. P., and Que, L., Jr. (2005) The 2-His-1-carboxylate facial triad: A versatile platform for dioxygen activation by mononuclear non-heme iron(II) enzymes, *J. Biol. Inorg. Chem. 10*, 87−93.
8. Que, L., Jr., and Ho, R. Y. N. (1996) Dioxygen Activation by Enzymes with Mononuclear Non-Heme Iron Active Sites, *Chem. Rev. 96*, 2607−2624.
9. Chen, V. J., Orville, A. M., Harpe, M. R., Frolik, C. A., Surerus, K. K., Münck, E., and Lipscomb, J. D. (1989) Spectroscopic Studies of Isopenicillin N Synthase, *J. Biol. Chem. 264*, 21677−21681.
10. Scott, R. A., Wang, S. K., Eidsness, M. K., Kriauciunas, A., Frolik, C. A., and Chen, V. J. (1992) X-ray Absorption Spectroscopic Studies of the High-Spin Iron(II) Active Site of Isopenicillin N Synthase: Evidence for Fe-S Interaction in the Enzyme-Substrate Complex, *Biochemistry 31*, 4596−4601.
11. Randall, C. R., Zang, Y., True, A. E., Que, L., Jr., Charnock, J. M., Garner, C. D., Fujishima, Y., Schofield, C. J., and Baldwin, J. E. (1993) X-ray Absorption Studies of the Ferrous Active Site of Isopenicillin N Synthase and Related Model Complexes, *Biochemistry 32*, 6664−6673.
12. Roach, P. L., Clifton, I. J., Fülöp, V., Harlos, K., Barton, G. J., Hajdu, J., Andersson, I., Schofield, C. J., and Baldwin, J. E. (1995) Crystal structure of isopenicillin N synthase is the first from a new family of enzymes, *Nature 375*, 700−704.
13. Burzlaff, N. I., Rutledge, P. J., Clifton, I. J., Hensgens, C. M. H., Pickford, M., Adlington, R. M., Roach, P. L., and Baldwin, J. E. (1999) The reaction cycle of isopenicillin N synthase observed by X-ray diffraction, *Nature 401*, 721−724.
14. Long, A. J., Clifton, I. J., Roach, P. L., Baldwin, J. E., Schofield, C. J., and Rutledge, P. J. (2003) Structural studies on the reaction of isopenicillin N synthase with the substrate analogue δ-(L-α-aminoadipoyl)-L-cysteinyl-D-α-aminobutyrate, *Biochem. J. 372*, 687−693.
15. Elkins, J. M., Rutledge, P. J., Burzlaff, N. I., Clifton, I. J., Adlington, R. M., Roach, P. L., and Baldwin, J. E. (2003) Crystallographic studies on the reaction of isopenicillin N synthase with an unsaturated substrate analogue, *Org. Biomol. Chem. 1*, 1455−1460.
16. Long, A. J., Clifton, I. J., Roach, P. L., Baldwin, J. E., Rutledge, P. J., and Schofield, C. J. (2005) Structural Studies on the Reaction of Isopenicillin N Synthase with the Truncated Substrate Analogues δ-(L-α-aminoadipoyl)-L-cysteinyl-glycine and δ-(L-α-aminoadipoyl)-L-cysteinyl-D-alanine, *Biochemistry 44*, 6619−6628.
17. Daruzzaman, A., Clifton, I. J., Adlington, R. M., Baldwin, J. E., and Rutledge, P. J. (2006) Unexpected Oxidation of a Depsipeptide Substrate Analogue in Crystalline Isopenicillin N Synthase, *ChemBioChem 7*, 351−358.
18. Kreisberg-Zakarin, R., Borovok, I., Yanko, M., Frolow, F., Aharonowitz, Y., and Cohen, G. (2000) Structure−function studies of the non-heme iron active site of isopenicillin N synthase: Some implications for catalysis, *Biophys. Chem. 86*, 109−118.
19. Borovok, I., Landman, O., Kreisberg-Zakarin, R., Aharonowitz, Y., and Cohen, G. (1996) Ferrous Active Site of Isopenicillin N Synthase: Genetic and Sequence Analysis of the Endogenous Ligands, *Biochemistry 35*, 1981−1987.
20. Sim, T.-S., and Loke, P. (2000) Molecular studies on isopenicillin N synthase, *Appl. Microbiol. Biotechnol. 54*, 1−8.
21. Solomon, E. I., Brunold, T. C., Davis, M. I., Kemsley, J. N., Lee, S.-K., Lehnert, N., Neese, F., Skulan, A. J., Yang, Y. S., and Zhou, J. (2000) Geometric and Electronic Structure/Function Correlations in Non-Heme Iron Enzymes, *Chem. Rev. 100*, 235−349.
22. Brown, C. D., Neidig, M. L., Neibergall, M. B., Lipscomb, J. B., and Solomon, E. I. (2007) VTVH-MCD and DFT Studies of Thiolate Bonding to $\{FeNO\}^7/\{FeO2\}^8$ Complexes of Isopenicillin N Synthase: Substrate Determination of Oxidase versus Oxygenase Activity in Nonheme Fe Enzymes, *J. Am. Chem. Soc. 129*, 7427−7438.
23. Baldwin, J. E., Adlington, R. M., Moroney, S. E., Field, L. D., and Ting, H.-H. (1984) Stepwise Ring-Closure in Penicillin Biosynthesis: Initial β-Lactam Formation, *J. Chem. Soc., Chem. Commun*., 984−986.
24. Wirstam, M., and Siegbahn, P. E. M. (2000) A Mechanistic Study of Isopenicillin N Formation Using Density Functional Theory, *J. Am. Chem. Soc. 122*, 8539−8547.
25. Baldwin, J. E., and Abraham, E. (1988) The Biosynthesis of Penicillins and Cephalosporins, *Nat. Prod. Rep. 5*, 129−145.
26. Bassan, A., Borowski, T., and Siegbahn, P. E. M. (2004) Quantum chemical studies of dioxygen activation by mononuclear non-heme iron enzymes with the 2-His-1-carboxylate facial triad, *Dalton Trans. 20*, 3153−3162.
27. Bassan, A., Blomberg, M. R. A., Borowski, T., and Siegbahn, P. E. M. (2006) Theoretical studies of enzyme mechanisms involving high-valent iron intermediates, *J. Inorg. Biochem. 100*, 727−743.
28. Kriauciunas, A., Frolik, C. A., Hassell, T. C., Skatrud, P. L., Johnson, M. G., Holbrok, N. I., and Chen, V. J. (1991) The Functional Role of Cysteines in Isopenicillin N Synthase, *J. Biol. Chem. 266*, 11779−11788.
29. Frisch, M. J., Trucks, G. W., Schlegel, H. B., Scuseria, G. E., Robb, M. A., Cheeseman, J. R., Montgomery, J. A., Jr., Vreven, T., Kudin, K. N., Burant, J. C., Millam, J. M., Iyengar, S. S., Tomasi, J., Barone, V., Mennucci, B., Cossi, M., Scalmani, G., Rega, N., Petersson, G. A., Nakatsuji, H., Hada, M., Ehara, M., Toyota, K., Fukuda, R., Hasegawa, J., Ishida, M., Nakajima, T., Honda, Y., Kitao, O., Nakai, H., Klene, M., Li, X., Knox, J. E., Hratchian, H. P., Cross, J. B., Bakken, V., Adamo, C., Jaramillo, J., Gomperts, R., Stratmann, R. E., Yazyev, O., Austin, A. J., Cammi, R., Pomelli, C., Ochterski, J. W., Ayala, P. Y., Morokuma, K., Voth, G. A., Salvador, P., Dannenberg, J. J., Zakrzewski, V. G., Dapprich, S., Daniels, A. D., Strain, M. C., Farkas, O., Malick, D. K., Rabuck, A. D., Raghavachari, K., Foresman, J. B., Ortiz, J. V., Cui, Q., Baboul, A. G., Clifford, S., Cioslowski, J., Stefanov, B. B., Liu, G., Liashenko, A., Piskorz, P., Komaromi, I., Martin, R. L., Fox, D. J., Keith, T., Al-Laham, M. A., Peng, C. Y., Nanayakkara, A., Challacombe, M., Gill, P. M. W., Johnson, B., Chen, W., Wong, M. W., Gonzalez, C., and Pople, J. A. (2004) *Gaussian 03*, revision C.02, Gaussian Inc., Wallingford, CT.
30. Becke, A. D. (1993) Density-functional thermochemistry. III. The role of exact exchange, *J. Chem. Phys. 98*, 5648−5652.
31. Siegbahn, P. E. M. (2006) The performance of hybrid DFT for mechanisms involving transition metal complexes in enzymes, *J. Biol. Inorg. Chem. 11*, 695−701.
32. Noodleman, L., and Case, D. A. (1992) Density-Functional Theory of Spin Polarization and Spin Coupling in Iron-Sulfur Clusters, *Adv. Inorg. Chem. 38*, 423−470.
33. Cances, E., Mennucci, B., and Tomasi, J. (1997) A new integral equation formalism for the polarizable continuum model: Theoretical background and applications to isotropic and anisotropic dielectrics, *J. Chem. Phys. 107*, 3032−3041.
34. Lundberg, M., and Morokuma, K. (2007) Protein Environment Facilitates O_2 Binding in Non-Heme Iron Enzyme. An Insight from ONIOM Calculations on Isopenicillin N Synthase (IPNS), *J. Phys. Chem. B 111*, 9380−9389.
35. Bassan, A., Blomberg, M. R. A., and Siegbahn, P. E. M. (2003) Mechanism of Dioxygen Cleavage in Tetrahydrobiopterin-Dependent Amino Acid Hydroxylases, *Chem.—Eur. J. 9*, 106−114.
36. Wirstam, M., Lippard, S. J., and Friesner, R. A. (2003) Reversible Dioxygen Binding to Hemerythrin, *J. Am. Chem. Soc. 125*, 3980−3987.

37. Blomberg, M. R. A., and Siegbahn, P. E. M. (1997) A comparative study of high-spin manganese and iron complexes, *Theor. Chem. Acc. 97*, 72−80.
38. Frey, P. A., Hegeman, A. D., and Reed, G. H. (2006) Free Radical Mechanisms in Enzymology, *Chem. Rev. 106*, 3302−3316.
39. Borowski, T., Bassan, A., and Siegbahn, P. E. M. (2004) A Hybrid Density Functional Study of O−O Bond Cleavage and Phenyl Ring Hydroxylation for a Biomimetic Non-Heme Iron Complex, *Inorg. Chem. 43*, 3277−3291.
40. Borowski, T., Bassan, A., and Siegbahn, P. E. M. (2004) Mechanism of Dioxygen Activation in 2-Oxoglutarate-Dependent Enzymes: A Hybrid DFT Study, *Chem.−Eur. J. 10*, 1031−1041.
41. Borowski, T., Bassan, A., and Siegbahn, P. E. M. (2004) 4-Hydroxyphenylpyruvate Dioxygenase: A Hybrid Density Functional Study of the Catalytic Reaction Mechanism, *Biochemistry 43*, 12331−12342.
42. Rohde, J. U., In, J.-H., Lim, M. H., Brennessel, W. W., Bukowski, M. R., Stubna, A., Münck, E., Nam, W., and Que, L., Jr. (2003) Crystallographic and Spectroscopic Characterization of a Nonheme Fe(IV)═O Complex, *Science 299*, 1037−1039.
43. Riggs-Gelasco, P. J., Price, J. C., Guyer, R. B., Brehm, J. H., Barr, E. W., Bollinger, J. M., and Krebs, C. (2004) EXAFS Spectroscopic Evidence for an Fe═O Unit in the Fe(IV) Intermediate Observed during Oxygen Activation by Taurine:α-Ketoglutarate Dioxygenase, *J. Am. Chem. Soc. 126*, 8108−8109.
44. Price, J. C., Barr, E. W., Tirupati, B., Bollinger, J. M., and Krebs, C. (2003) The First Direct Characterization of a High-Valent Iron Intermediate in the Reaction of an α-Ketoglutarate-Dependent Dioxygenase: A High-Spin Fe(IV) Complex in Taurine/α-Ketoglutarate Dioxygenase (TauD) from *Escherichia coli*, *Biochemistry 42*, 7497−7508.
45. Noack, H., and Siegbahn, P. E. M. (2007) Theoretical investigation on the oxidative chlorination performed by a biomimetic non-heme iron catalyst, *J. Biol. Inorg. Chem.* DOI 10.1007/s00775-007-0284-0.

BI701577Q